Impact of Applied Potential on the Facet Ratio and Size of Ir and Cu Catalysts

Peshala K. Jayamaha and Lichang Wang*

School of Chemical and Biomolecular Sciences, Southern Illinois University Carbondale, Carbondale, IL 62901, USA

Abstract

The surface energy of a catalyst material is important for understanding the fundamental behavior of nanoparticles and bulk crystals, particularly in terms of activity, selectivity, durability, and stability. Computational studies of electrocatalysts provide valuable insight into the stability of electrode surfaces under realistic environments, including solid/liquid interfaces. In this work, we model the electrode/solid surface using the density functional theory (DFT), and electrolyte/liquid using the implicit solvation model. Importantly, we examined the surface energies of low-index facets of Ir and Cu crystals in an aqueous electrolyte as a function of applied electrode potential. The results show that each surface facet of the neutral surface belongs to an initial potential which is called the potential of zero charge (PZC). Both Ir and Cu (111) facets have higher PZC values relative to other studied facets. Ir and Cu (111) facets exhibit the most stable surfaces with low surface energy profiles within the range of applied potential, while (110) facets show the lowest stability for electrocatalyst applications. This study shows that the surface energies are highly sensitive to the applied potential and leads to the change in particle size and facet ratio under the applied potentials.

*Corresponding author: lwang@chem.siu.edu

1. Introduction

The demand for energy is continuously growing with the increasing global population. Fossil fuels, the major source of energy supply for global demand, cause mass CO_2 emissions and hence climate change. So, it is very important to make the shift toward sustainable and efficient energy sources.[1] Electrocatalysis has shown a significant advancement in sustainable and efficient energy production via applications such as fuel cells. Fuel cells produce electricity directly from chemical energy, promising a clean energy source. The main electrochemical conversions in fuel cell applications involve the molecules present in the earth's atmosphere such as CO_2, O_2, and H_2O.[2] The most prominent reaction schemes involved in this energy transformation are the oxygen evolution reaction (OER),[3-5] hydrogen evolution reaction (HER),[6-8] oxygen reduction reaction (ORR),[9] hydrogen oxidation reaction (HOR), CO_2 reduction reaction (CO_2RR),[10-31] water splitting,[32, 33] and the production of environmentally friendly byproducts.[34] Recently, renewable energy materials, such as ethanol,[35-39] has attracted a great attention for ethanol fuel cells, where ethanol oxidation reaction (EOR) has been extensively studied.[26, 40-54] As clean energy fuel hydrogen is mostly produced from natural gas, green production of hydrogen has been active area of research as well.[55-58] To optimize the performance and applications of electrocatalysis, the performances of the catalyst materials should be studied under different reaction conditions.[59-63] Efficient catalyst materials used as electrodes in fuel cells can enhance the electrochemical reaction that occurs in the electrode-electrolyte interface. During the operation of fuel cells, maintaining the electrode surface's stability throughout the process is very important.

Surface energy describes the fundamental material properties in terms of stability, selectivity, shape, growth, and surface structure. Surface energy is the energy required to create a new surface and it is always a positive quantity.[64,65] The degree of coordinative unsaturation of the surface

atoms influences the surface energy of a particular metal, more reactive surfaces possess higher surface energies. Surface energy is not a fixed quantity, it depends on the surrounding environment of the material. The experimental determination of this quantity is difficult since it requires measuring the surface tension at the melting temperature of the metal.[66] However theoretical surface energy determination using computational tools,[67-70] such as density functional theory (DFT) calculations, is easy, less expensive, and useful in studying the relative stability of surface facets commonly used in catalysis,[71-78] which is critical in the studies[79, 80] and applications[81, 82] of organic small molecules.

McCrum and his co-workers have demonstrated computationally that the surface energies of the low index facets of Pt are impacted by the aqueous environment as a function of different applied potentials under different adsorbates.[83] They performed simulations to calculate the potential dependent-surface energies of Pt (111), Pt (110) and Pt (100) with varying the coverages of adsorbed hydrogen, hydroxide, and coadsorbed water, and oxygen. They have performed their surface energy calculations relative to the bare surface energy values taken from literature. Those bare surface energies taken from literature[65] didn't account for the solvent effect on the crystal surfaces. McCrum's work has considered the bare surface energy as a potential independent quantity. They found that Pt (111) is the most stable as a bare surface compared to the other two facets, while Pt (100) and Pt (110) become more stable in the presence of strong adsorption of hydrogen and hydroxide at specific potentials. Their results have shown that potentials above the 0.7 V_{RHE} drives the formation of lower surface energy facets of Pt (110) and Pt (100) on reduction of surface oxide. In this work we calculated the bare surface energies as a function of applied potential while considering the solvent effect on bare surfaces to understand the effect of applied potential on catalyst surface prior to the occurrence of an electrochemical reaction.

Mathew et al. has shown the utility of implicit solvation model for studying electrode surfaces energies as a function of applied potential, with including the effect of electrolyte using VASPsol simulation.[84] Their work has shown the sensitivity of surface energies of different facets of Cu crystals towards the applied potential and follow different trends. They found that Cu (111) facet exhibits the lowest surface energy over potential from -2.0 to 3.0 V. Surface energies of Cu facets have been studied there relative to the (111) surface energy as a function of applied potential. At negative potentials, (111) facet dominate the crystal shape, with increasing the potential ratio of (100) to (111) surface energies are getting decreased according to their simulation. When the applied potential was around -0.56 V, that crystal shape transition occurred. Simulation has demonstrated further increase in potential has led to an increase in the area of the (100) facets. Most of catalytic studies use Cu(111) surface,[85-87] as model catalyst surface to investigate adsorption and reactions. There are studies on the investigation of Cu(100).[88] It would be interesting to investigate the change of facet and size of catalyst nanoparticles under various applied potentials.

Studies for surface energy calculations have been performed to investigate the surface energies of industrially valuable metals.[89] Computational studies have conducted to investigate the surface energy profiles of low-index facets of metals like Al, Pd, Pt, Au, Li, and Ti in terms of the slab thickness for designing catalyst materials used in nanoscale devices.[65,90,91] Studies have shown that the effect of applied potential on stabilization and destabilization of the adsorption species and intermediate species on electrode surface during the electrocatalytic process.[92]

In this work, we performed DFT calculations using the Vienna *ab initio* simulation package (VASP) to obtain the surface energies of anode materials, which are used in fuel cells as a function of applied potential. The solvent effect also plays a major role in electrocatalysis. To account for

the solvent effect in the calculations we performed the VASPsol calculations which include the implicit solvation model.[93, 94,95] The effect from the mobile ions in the electrolyte is included through the linearized Poisson-Boltzmann equation.[84,96] To study the effect of applied potential on surface energies of catalyst, we used the constant electrode potential model (CEP).[97,98] This work will provide benchmark results for future computational studies when other important factors, such as explicit solvent molecules[94, 99-102] and surface defects,[103, 104] are included.

Specifically, we performed a theoretical investigation of the surface energy profiles of Ir and Cu (111), (110), (100) facets by varying applied potential to investigate the anode material stability for fuel cell applications. The surface energies of Ir and Cu are very important, as these metals are widely used in heterogeneous electrocatalytic reactions. In this work, the implicit solvation model provides the ionic environment (electrolyte) and the electrochemical interfacial system under applied external potential. Hence, we can determine the stable surface facets for each applied potential. Most of the theoretical calculations predict the surface energies for metals while neglecting the solvent effect and applied potential effect on the bare metal surfaces. Using the results of surface energy, we attempted to understand the ratio of different surface facets and size of nanoparticles at various applied potentials, as both factors, ratio of facets and size of nanoparticles play important roles in catalysis due to the different electronic properties.[105-116] Here we hope to bridge the gap between theoretical calculations and practical situations of electrocatalysts/electrode stability in terms of surface energy, including electrolyte and applied potential impact on bare surfaces. This will accelerate the development of electrocatalysts and enhance the potential of sustainable energy conversion technologies using electrocatalysis.

2. Computational Method

In this work, all DFT calculations were performed using the Vienna *ab initio* simulation package (VASP).[117,118] The projector augmented wave (PAW) pseudopotentials were used to describe the ionic interactions of the valence electrons with ionic cores.[119] A plane-wave basis set was used with a cut-off energy of 400 eV. The generalized gradient approximation Perdew-Bruke-Ernzerhof (GGA-PBE) functionals were employed to describe the exchange-correlation interactions.[120] We utilized 1×1 Ir (111), (110), (100) and Cu (111), (110), (100) surfaces with five-layer slab models. The top three layers were relaxed, and the bottom two layers were fixed in the geometry optimization. The slab was separated by a 15 Å to avoid periodic interactions. For Ir (111), (110), (100) surfaces, 5×5×1,6×5×1,6×6×1 and for Cu (111), (110), (100) surfaces, 9×9×1,7×5×1,7×7×1 Monkhorst-Pack mesh k-space sampling grids[121] were used generated using VASPKIT[122] for ionic relaxation respectively. We used these periodic slab models to calculate the surface energies. Geometry optimization was allowed until the maximum force was less than 0.02 eV/Å and the electronic self-consistency cycles were less than 10^{-5} eV.

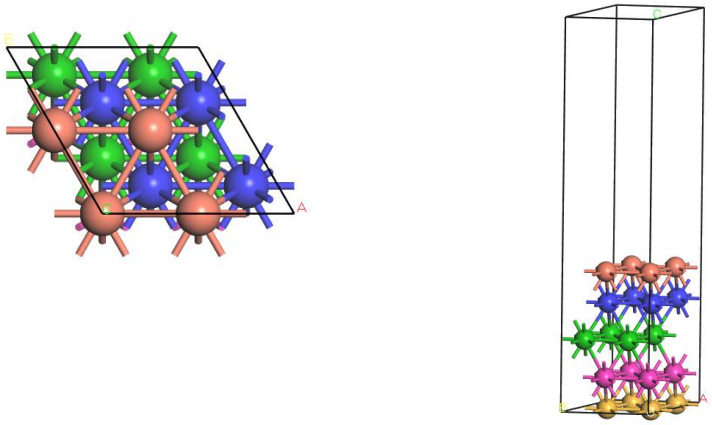

Figure 1. The top view (left) and side view with 5 layers slab (right) of the Cu (111)

We used the VASPsol,[93, 123,93] a software package that introduces solvation into VASP within a self-consistent continuum model to simulate the implicit water environment. The relative permittivity of the bulk solvent, the width of the dielectric cavity, and the cutoff charge density were 78.4, 0.6, and 0.0025. We employed an electrolyte (aqueous solution) that consisted of monovalent cations and anions, both at a concentration of 1M. At room temperature, the electrolyte demonstrates a Debye length of λ_D = 3.00 Å with employing the default values for achieving effective surface tension and cavity shape function.[124] More details can be found in the recent review and work on the implicit solvation methods.[125-128] Recent development of dealing with interface is also interesting.[129-136]

To apply a constant potential(U) to catalytic models, we adjust the number of electrons in each system to make the changes in Fermi level and then determine the corresponding potential. The applied potential is calculated with reference to the standard hydrogen electrode (SHE) from the Fermi energy in eq. (1).[98,96]

$$U = \frac{-\varepsilon_F - \phi_{SHE}}{e} \quad (1)$$

where ε_F is the Fermi energy and ϕ_{SHE} is the thermodynamic work function of the SHE. The theoretically predicted value for the ϕ_{SHE} is -4.30 eV for PBE functional.[96] Here we set the applied potential from 0.1 V to 1.5 V and calculated the surface energy as a function of applied potential.

Surface energies (E_{surf}) were calculated for surface slabs using eqn. (2) for bare surface and surface energy after applying a constant potential were calculated using eqn. (3).

$$E_{surf} = \frac{E_{slab} - nE_{bulk}}{2A} \quad (2)$$

$$E_{surf} = \frac{E_{slab} - nE_{bulk} + xU}{2A} \quad (3)$$

where E_{slab} and E_{bulk} are the total energy of the slab model and energy per atom in the bulk crystal. A is the area at the top of the slab, n, x and U denote the total number of atoms in the slab model, number of electrons added to determine the corresponding potential and applied potential respectively.

3. Results

DFT calculations were performed to obtain the surface energies of low index facets (111,110, and 100) of Ir and Pt in an aqueous environment, as a function of applied potential. We selected Ir and Cu as these metals are widely used as electrode materials in fuel cells and electrocatalysis. Studies have been performed to find the surface energies of catalytically active metals,[66,89] though few studies have focused on surface energy changes as applied potential. In one of our previous works,[137] we performed the DFT calculations to find the surface energies of trimetallic PtPdCu nanoalloy under the adsorbed O species with applied potentials. Here we determined the surface energies of Ir and Cu without any adsorbed species to investigate the anode material stability. Before performing DFT calculations under applied potentials, we calculated surface energies of Cu(111), Pd(111), Pt(111), and Ir(111). The results are summaried in Table 1 together with the data in literature.

Table 1: Bare surface energies of (111) Cu, Pd, Pt, and Ir. For comparison with our preliminary results (present) in surface energy calculation, we have included some theoretical results from the literature.

Metal	Bare surface energy / (J/m^2)	
	Present	Literature
Cu (111)	1.32	1.29[138], 1.97[139]
Pd (111)	1.30	1.31[65]
Pt (111)	1.50	1.49[65]
Ir (111)	2.23	2.26[140]

As the data in Table 1 has shown, the DFT results obtained in this work and those from literature are almost similar,[65,138,140] except for one. Tafreshi et al. have performed calculations using DFT-D2 method for accounting the dispersion interactions.[139] Similar results are seen here for the bare surface energies for Cu (111), Pd (111), Pt (111), and Ir (111).

3.1 Surface Energies of Ir and Cu Catalysts under Applied Potentials vs SHE

Figure 2 shows the surface energies for low index facets of Ir and Cu as function of applied potential vs the standard hydrogen electrode (SHE) calculated with the implicit electrolyte model.

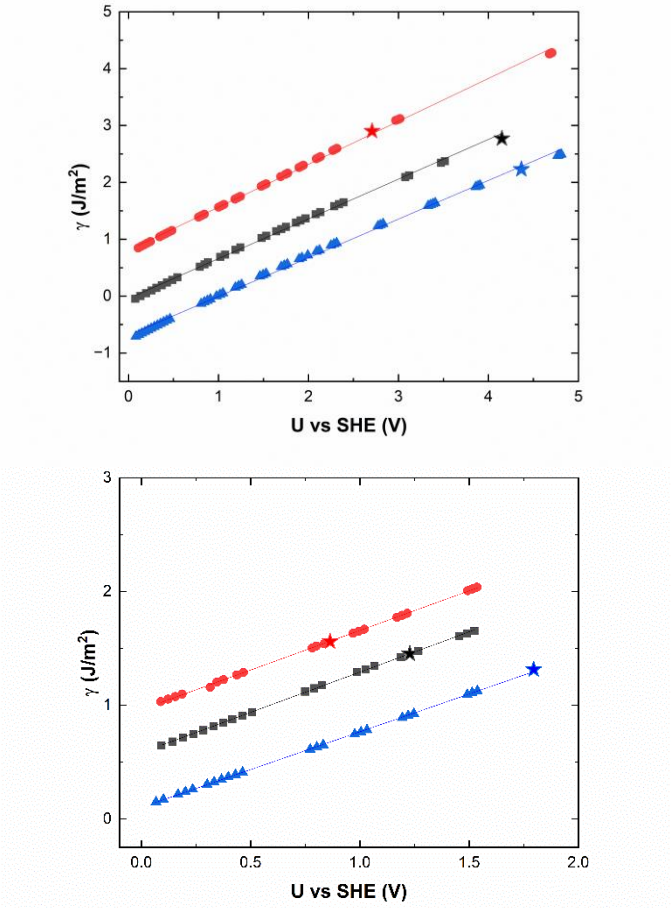

Figure 2. Surface energy as a function of applied potential on Ir (111), Ir (110), and Ir (100) (top), and Cu (111), Cu (110), and Cu (100) (bottom). Star marks define the potential of neutral metal surfaces.

Both panels in Figure 2 show the same trend for surface energies with the applied potentials. We applied electrode potentials, by changing the number of electrons and then shifting the Fermi level of our models in our simulation. The studied potential ranges were 0.1-4.8 V for Ir and 0.1 – 1.5 V for Cu. We selected these potential ranges based on the potentials at neutral surfaces of metals. (111) surface energies for Ir and Cu show the lowest surface energies, define the most stable surfaces. For Ir (111) surface it shows negative values for the surface energies up to the applied potential was 0.8 V. Once we increase the applied potential from 0.8 V onwards, surface energy increases as the potential increased for Ir (111). In both metals (110) surfaces show the highest surface energies within the applied potential ranges. According to the results, Ir and Cu (110) surfaces are generally indicative of the least stable surfaces in an aqueous environment under the applied potentials. These results depict that when using the Ir and Cu as the electrocatalyst materials in reaction systems and apply the low potentials (0.1- 0.9 V), crystal stabilizes with the (111) and (100) surfaces. Hence these two facets will facilitate the effective catalytic reactions. The applied potential can make structural changes in crystals according to the results. In the case of both Ir and Cu, increasing the applied potential leads to dissolving the (110) facet so easily relative to the (111) and (100) facets as higher surface energy profiles. These low-energy surfaces will provide more productive outcomes during electrocatalysis reactions relative to other facets with their stability. This surface energy calculation as a function of applied potential without any catalytic reaction and external species will help to expand the studying scope of efficiency in electrocatalysis. These results will help in designing nanoparticles for electrocatalysts. These results may help guide the setup reaction conditions for the electrocatalytic processes, and design and develop the shape-controlled nanoparticles for electrocatalysis in sustainable energy production.

3.2 Surface Energies of Ir and Cu Catalysts under Applied Potentials vs PZC

In addition to the surface energy as a function of applied potential vs SHE, we computed the potential of zero charges (PZC) of all the facets being studied here for the surface energy calculations. The PZC of the electrode is the potential of neutral metal electrode and it is defined by the fermi energy measured relative to the reference electrode.[84,123] Both theoretical and experimental determination[141] of PZC values are especially important in nanoparticle designing. These values for Cu (111), (110), and (100) are 1.314, 0.864, and 1.228 V respectively. The PZC values for Ir (111), (110), and (100) are 4.366, 2.707, and 4.149 V respectively. The highest potential at the neutral surface is obtained from (111) facet in both cases. Higher potentials can cause metal dissolution.[142] In our study, higher potential at Ir (111) neutral surface in an aqueous environment means that it is more prone to dissolution and will not function as a durable electrocatalyst. Dissolution is a very important factor when designing nanoparticles. So, determination of PZC values is very important in this type of study. Mathew et al. also have performed DFT calculations using VASPsol, and their study found that the highest PZC value belongs to the Cu (111), next is Cu (111), and the lowest PZC belongs to Cu (100) facet.[84] It is the same trend we found in our calculations as well.

Figure 3 shows the surface energy, γ, as a function of the applied potential vs PZC. For both metals, with the increase in PZC, surface energy also increased. The PZC values of Cu show relatively parallel pattern in surface energy profiles. Ir (100) and Ir (110) surface energies are overlapped around 1V.

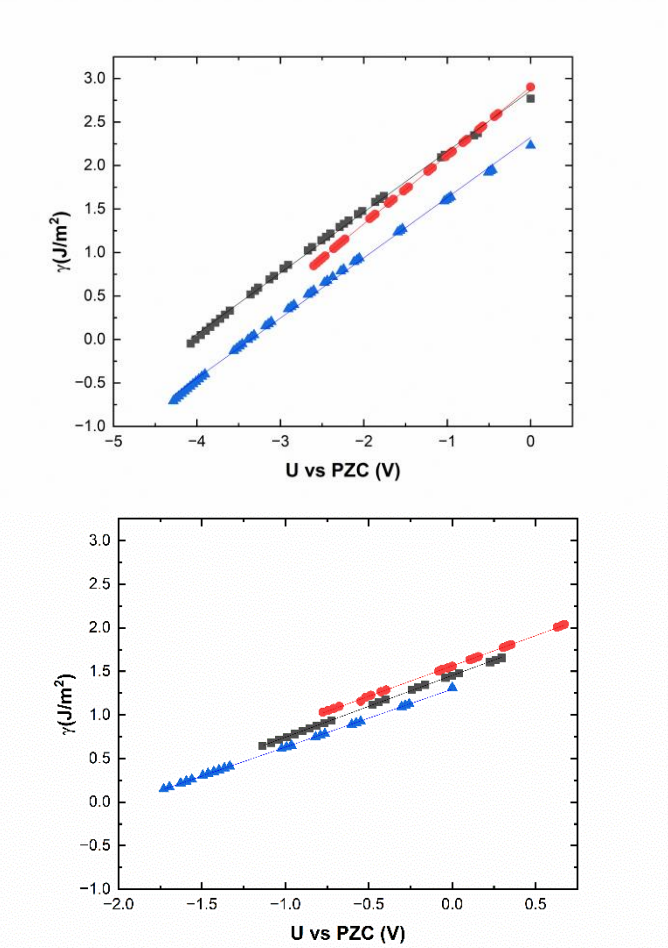

Figure 3. Surface energy as a function of applied potential vs. PZC on Ir (111), Ir (110), and Ir (100) (top), and Cu (111), Cu (110), and Cu (100) (bottom).

The surface energies of the metals can affect the shape of crystals and factors affecting the surface energy is important catalysis. To illustrate the impact of applied potential on electrode material implicit solvent calculations provide a significant insight. The applied potential can cause changes in equilibrium shape of crystals, dissolution of surfaces.

3.3 Facet Ratio and Size of Ir and Cu Catalysts under Applied Potentials vs SHE

Under electrochemical environments, surface structures, such as facet ratio, and size of catalysts may change depending on reactions taking place, pH, and applied potential. Here we investigate the critical applied potential vs SHE that may lead to the size and facet ratio changes.

To understand the facet ratio change, we plot in Figure 4 the ratio of surface energies of Ir and Cu.

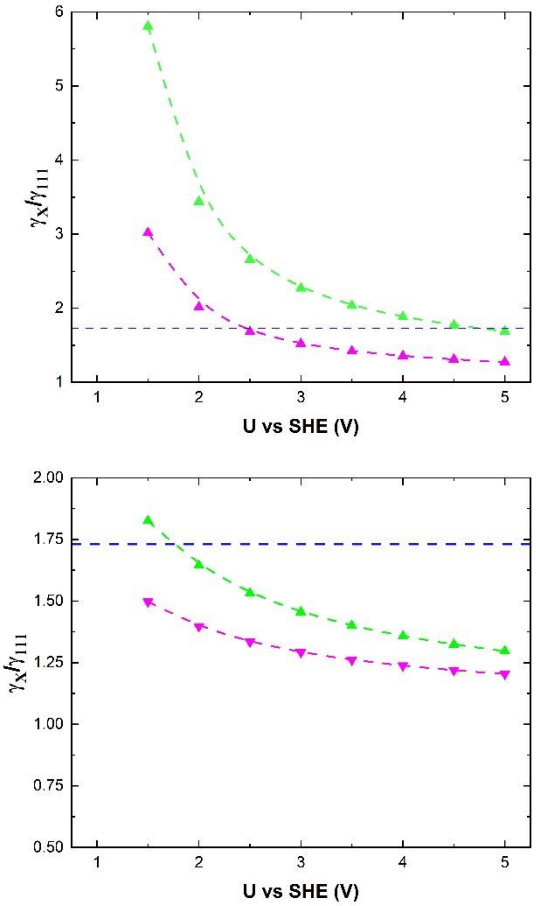

Figure 4. Surface energy ratio to (111) as a function of applied potential vs. SHE on Ir (top) and Cu (bottom). Green lines are (110)/(111) and pink are 100/111.

The dashed lines are at ratio of 1.73 in Figure 4 and it indicates the changes of facets. For Ir catalysts, once the applied potentials are in the range of <2.5 V vs SHE, Ir(100) is more abundant than Ir(111). On the other hand, For Cu catalysts, the dominant facet within the range of applied potentials studied here is (111). In terms of catalyst size change, it takes place for Ir catalysts when the applied potential is below 1 V (see Figure 1). Cu catalysts are rather stable under the applied potentials studied here.

4. Conclusions

DFT calculations were performed to model the implicit solvent environment using the VASPsol solvation model to find the surface energies of Ir and Cu (111), (110), and (100) facets as a function of applied potential. We performed the calculations to find the surface energies with applied potentials as surface energies cause the change the shape of the crystal. The highest PZC values belong to the Ir (111) and Cu (111) facets, implying that these facets are more prone to dissolution prior to applying the electrode potentials relative to (110) and (100) facets. For both Ir and Cu (111) facets have shown the lowest surface energies with promising stable surfaces. The results imply that surface energies are sensitive to the applied potentials, and hence promising opportunity to control the shape of nanocrystals with the external potential. These results highlight the importance of studying the shape of catalyst material used in electrocatalysis with applied potential in the presence of electrolyte prior to the redox reaction occurring. This computational electrochemistry simulation will be useful in designing and modelling electrode nanomaterials using Cu and Ir catalysts.

Acknowledgements

The research was partly supported by the Illinois Soybean Center.

References

1. N. Govindarajan, G. Kastlunger, H. H. Heenen and K. Chan, *Chem. Sci.*, 2022, **13**, 14-26.
2. Z. W. Seh, J. Kibsgaard, C. F. Dickens, I. Chorkendorff, J. K. Nørskov and T. F. Jaramillo, *Science*, 2017, **355**, eaad4998.
3. *Nat. Commun.*, 2023, **14**, 4228.
4. Y. Ding, W. Liu, Z. Xu and Z. Duan, *J. Mater. Chem. A*, 2024, **12**, 20317-20326.
5. W. Zhu, Q. Sun, M. Ma, F. Liao, Q. Shao, H. Huang, K. Feng, D. Gao, J. Chen, H. Yang, P. Yu, J. Zhong, T. Cheng, M. Shao, Y. Liu and Z. Kang, *Nano Energy*, 2024, **131**, 110280.
6. S. Wang, G. Feng, W. Xu, W. Li and J. Wang, *Comput. Mater. Sci.*, 2023, **229**, 112397.
7. P.-J. Lina, C.-H. Yeh and J.-C. Jiang, *RSC Adv.*, 2021, **11**, 36257-36264.
8. X. Huang, J. Xu, J. Gao, Y. Cui, X. Xu and S. Wang, *J. Phys. Chem. C*, 2024, **128**, 11278–11288.

9. J. T. Bender, R. Y. Sanspeur, A. E. Valles, A. K. Uvodich, D. J. Milliron, J. R. Kitchin and J. Resasco, *ACS Energy Lett.*, 2024, **9**, 4724–4733.
10. X. Bai, X. Zhao, Y. Zhang, C. Ling, Y. Zhou, J. Wang and Y. Liu, *J. Am. Chem. Soc.*, 2022, **144**, 17140-17148.
11. S. Osella and W. A. G. III, *J. Am. Chem. Soc.*, 2023, **145**, 21319-21329.
12. Q. Zhao, J. M. P. Martirez and E. A. Carter, *PNAS*, 2022, **119**, e2202931119.
13. P. Wang, H. Yang, Y. Xu, X. Huang, J. Wang, M. Zhong, T. Cheng and Q. Shao, *ACS NANo*, 2021, **15**, 1039-1047.
14. J. A. Gauthier, Z. Lin, M. Head-Gordon and A. T. Bell, *ACS Energy Lett.*, 2022, **7**, 1679–1686.
15. W.-Y. Lin, Z.-X. Chen, H. Xiong, H.-C. Li, Y.-S. Ho, C.-T. Hsieh, Q. Lu and M.-J. Cheng, *ACS Catal.*, 2023, **13**, 11697–11710.
16. C. Zhao and H. Xu, *J. Phys. Chem. Lett.*, 2023, **14**, 1928–1933.
17. R. M. Kowalski, A. Banerjee, C. Yue, S. G. Gracia, D. Cheng, C. G. Morales-Guio and P. Sautet, *J. Am. Chem. Soc.*, 2024, **146**, 20728–20741.
18. S.-Q. Xiang, J.-L. Shi, S.-T. Gao, W. Zhang and L.-B. Zhao, *ACS Catal.*, 2021, **11**, 2422–2434.
19. Q. Li, Y. Zhang, L. Shi, M. Wu, Y. Ouyang and J. Wang, *InfoMat*, 2021, **3**, 1285-1294.
20. Q. Zhao, J. M. P. Martirez and E. A. Carter, *J. Phys. Chem. Lett.*, 2022, **13**, 10282–10290.
21. S. Liu, Y. Li, D. Wang, S. Xi, H. Xu, Y. Wang, X. Li, W. Zang, W. Liu, M. Su, K. Yan, A. C. Nielander, A. B. Wong, J. Lu, T. F. Jaramillo, L. W. P. Canepa and Q. He, *Nat. Commun.*, 2024, **15**, 5080.
22. T.-C. Kuo, J.-W. Chou, M.-H. Shen, Z.-S. Hong, T.-H. Chao, Q. Lu and M.-J. Cheng, *J. Phys. Chem. C*, 2021, **125**, 2464–2476.
23. A. Das, S. C. Mandal, S. Das and B. Pathak, *J. Phys. Chem. C*, 2022, **126**, 21628–21637.
24. Q. Zhao and E. A. Carter, *J. Chem. Theory Comput.*, 2020, **16**, 6528–6538.
25. H. Yu, S. E. Weitzner, J. B. Varley, B. C. Wood and S. A. Akhade, *J. Phys. Chem. C*, 2023, **127**, 1789–1797.
26. Y.-L. Li, X.-L. Jiang, H. Cao, H.-Y. Zhao, J. Li and Y.-G. Wang, *ACS Catal.*, 2024, **14**, 9575–9585.
27. H. Yang, W. Zou, C. Zhang and A. Du, *ACS Appl. Mater. Interfaces*, 2024, **16**, 33688–33695.
28. Z. Zhang, W. Gee, P. Sautet and A. N. Alexandrova, *J. Am. Chem. Soc.*, 2024, **146**, 16119–16127.
29. X.-G. Zhang, Y. Zhao, S. Chen, S.-M. Xing, J.-C. Dong and J.-F. Li, *J. Chem. Phys.*, 2023, **158**, 094704.
30. F. Zhang, L. Gong, M. Liu, Y. Ying, Y. Cui, J. Shao, Y. Yu, A. Gao, J. Ma and L. Zhang, *Nano Energy*, 2024, **127**, 109699.
31. M. R. Fiorentin, F. Risplendi, C. Salvini, J. Zeng, G. Cicero and H. Jónsson, *J. Phys. Chem. Lett.*, 2024, **15**, 11538–11545.
32. S. Park, T. Jang, S. Choi, Y. H. Lee, K. H. Cho, M. Y. Lee, H. Seo, H. K. Lim, Y. Kim, J. Ryu, S. W. Im, M. G. Kim, J.-S. Park, M. Kim, K. Jin and S. H. Kim, *J. Am. Chem. Soc.*, 2023, **145**, 26632–26644.
33. W. Liu, Z. Duan and W. Wang, *J. Phys. Chem. C*, 2023, **127**, 5334–5342.
34. R. O'hayre, S.-W. Cha, W. Colella and F. B. Prinz, *Fuel cell fundamentals*, John Wiley & Sons, 2016.
35. K. Sun, M. Zhang and L. Wang, *Chem. Phys. Lett.*, 2013, **585**, 89-94.

36. R. Wu, K. Sun, Y. Chen, M. Zhang and L. Wang, *Surf. Sci.*, 2021, **703**, 121742.
37. R. Wu and L. Wang, *Comput. Mater. Sci.*, 2021, **196**, 110514.
38. R. Wu and L. Wang, *Chem. Phys. Lett.*, 2017, **678**, 196-202.
39. Z. Li, Y. Yan, S.-M. Xu, H. Zhou, M. Xu, L. Ma, M. Shao, X. Kong, B. Wang, L. Zheng and H. Duan, *Nat. Commun.*, 2022, **13**, 147.
40. B. Miao, Z. Wu, M. Zhang, Y. Chen and L. Wang, *J. Phys. Chem. C*, 2018, **122**, 22448-22459.
41. B. Miao, Z.-P. Wu, H. Xu, M. Zhang, Y. Chen and L. Wang, *Comput. Mater. Sci.*, 2019, **156**, 175-186.
42. Z.-P. Wu, B. Miao, E. Hopkins, K. Park, Y. Chen, H. Jiang, M. Zhang, C.-J. Zhong and L. Wang, *J. Phys. Chem. C*, 2019, **123**, 20853-20868.
43. H. Xu, B. Miao, M. Zhang, Y. Chen and L. Wang, *Phys. Chem. Chem. Phys.*, 2017, **19**, 26210-26220.
44. Z. Wu, M. Zhang, H. Jiang, C.-J. Zhong, Y. Chen and L. Wang, *Phys. Chem. Chem. Phys.*, 2017, **19**, 15444-15453.
45. B. Miao, Z. Wu, H. Xu, M. Zhang, Y. Chen and L. Wang, *Chem. Phys. Lett.*, 2017, **688**, 92-97.
46. R. Wu and L. Wang, *J. Phys. Chem. C*, 2020, **124**, 26953-26964.
47. R. Wu, K. R. Wiegand and L. Wang, *J. Chem. Phys.*, 2021, **154**, 054705.
48. R. Wu and L. Wang, *Chem. Phys. Impact*, 2021, **3**, 100040.
49. R. Wu and L. Wang, *J. Phys. Chem. C* 2022, **126**, 21650-21666.
50. R. Wu and L. Wang, *ChemPhysChem*, 2022, **23**, e202200132.
51. H. Tian, R. Zhu, P. Deng, J. Li, W. Huang, Q. Chen, Y.-Q. Su, C. Jia, Z. Liu, Y. Shen and X. Tian, *Small*, 2022, **18**, 2203506.
52. K. Barman, G. Askarova, R. Jia, G. Hu and M. V. Mirkin, *J. Am. Chem. Soc.*, 2023, **145**, 5786–5794.
53. Y. Guo, B. Li, S. Shen, L. Luo, G. Wang and J. Zhang, *ACS Appl. Mater. Interfaces*, 2021, **13**, 16602–16610.
54. H. Yu, N. Govindarajan, S. E. Weitzner, R. F. Serra-Maia, S. A. Akhade and J. B. Varley, *ChemPhysChem*, 2024, **25**, e202300959.
55. C. Wu, Z. Xiao, L. Wang, G. Li, X. Zhang and L. Wang, *Catal. Sci. Technol.*, 2021, **11**, 1965-1973.
56. C. Wu, L. Wang, Z. Xiao, G. Li and L. Wang, *Phys. Chem. Chem. Phys.*, 2020, **22**, 724-733.
57. C. Wu, L. Wang, Z. Xiao, G. Li and L. Wang, *Chem. Phys. Lett.*, 2020, **746**, 137229.
58. R. Wu, K. R. Wiegand, L. Ge and L. Wang, *J. Phys. Chem. C* 2021, **125**, 14275-14286.
59. A. Lu, Z.-P. Wu, B. Chen, D.-L. Peng, S. Yan, S. Shan, Z. Skeete, F. Chang, Y. Chen, H. Zheng, D. Zeng, L. Yang, A. Sharma, J. Luo, L. Wang, V. Petkov and C.-J. Zhong, *J. Mater. Chem. A*, 2018, **6**, 5143-5155.
60. H. Ooka, J. Huang and K. S. Exner, *Front. Energy Res.*, 2021, **9**, 654460.
61. J. Lim, C.-Y. Liu, J. Park, Y.-H. Liu, T. P. Senftle, S. W. Lee and M. C. Hatzell, *ACS Catal.*, 2021, **11**, 7568-7577.
62. J.-C. Liu, F. Luo and J. Li, *J. Am. Chem. Soc.*, 2023, **145**, 25264-25273.
63. A. J.-W. Wong, J. L. Miller and M. J. Janik, *Chem. Catal.*, 2022, **2**, 1362-1379.
64. Z. Łodziana, N.-Y. Topsøe and J. K. Nørskov, *Nat. Mater.*, 2004, **3**, 289-293.
65. N. E. Singh-Miller and N. Marzari, *Phys. Rev. B*, 2009, **80**, 235407.
66. W. Tyson and W. Miller, *Surf. Sci.*, 1977, **62**, 267-276.

67. B. W. J. Chen, L. Xu and M. Mavrikakis, *Chem. Rev.*, 2021, **121**, 1007-1048.
68. Z. Levell, J. Le, S. Yu, R. Wang, S. Ethirajan, R. Rana, A. Kulkarni, J. Resasco, D. Lu, J. Cheng and Y. Liu, *Chem. Rev.*, 2024, **124**, 8620-8656.
69. N. Abidi, K. R. G. Lim, Z. W. Seh and S. N. Steinmann, *WIRE Comput. Mol. Sci.*, 2021, **11**, e1499.
70. A. M. Patel, S. Vijay, G. Kastlunger, J. K. Nørskov and K. Chan, *J. Phys. Chem. Lett.*, 2021, **12**, 5193–5200.
71. R. Stumpf, *Surf. Sci.*, 2007, **601**, L115-L119.
72. X. Zhang, A. Chen, L. Chen and Z. Zhou, *Adv. Energy Mater.*, 2022, **12**, 2003841.
73. L. Miao, W. Jia, X. Cao and L. Jiao, *Chem. Soc. Rev.*, 2024, **53**, 2771-2807.
74. N. Abidi and S. N. Steinmann, *Current Opinion Electrochem.*, 2022, **33**, 100940.
75. Q. Li, Y. Ouyang, S. Lu, X. Bai, Y. Zhang, L. Shi, C. Ling and J. Wang, *Chem. Commun.*, 2020, **56**, 9937-9949.
76. Z. W. P. Sautet, *Angew. Chem. Int. Ed.*, 2022, **61**, e202210060.
77. Y. Li, G. Huang, Y. Jiang, C. Ma, Y. Lu, S. Wang and Y. Zou, *J. Phys. Chem. C*, 2023, **127**, 21989–21998.
78. Y. Guan, J. Kümper, S. D. Mürtz, S. Kumari, P. J. C. Hausoul, R. Palkovitt and P. Sautet, *Chem. Sci.*, 2024, **15**, 14485-14496.
79. T. Wang, C. Zhao, L. Zhang, T. Lu, H. Sun, C. N. Bridgmohan, K. C. Weerasinghe, D. Liu, W. Hu, W. Li, X. Zhou and L. Wang, *J. Phys. Chem. C*, 2016, **120**, 25263-25275.
80. T. Wang, K. C. Weerasinghe, P. C. Ubaldo, D. Liu, W. Li, X. Zhou and L. Wang, *Chem. Phys. Lett.*, 2015, **618**, 142-146.
81. H. Sun, D. Liu, T. Wang, P. Li, C. N. Bridgmohan, W. Li, T. Lu, W. Hu, L. Wang and X. Zhou, *Org. Electronics*, 2018, **61**, 35-45.
82. D. Y. Muleta, J. Song, W. Feng, R. Wu, X. Zhou, W. Li, L. Wang, D. Liu, T. Wang and W. Hu, *J. Mater. Chem. C*, 2021, **9**, 5093-5097.
83. I. T. McCrum, M. A. Hickner and M. J. Janik, *Langmuir*, 2017, **33**, 7043-7052.
84. K. Mathew, V. Kolluru, S. Mula, S. N. Steinmann and R. G. Hennig, *J. Chem. Phys.*, 2019, **151**, 234101.
85. L. Wang, Q. Ge and G. D. Billing, *Surf. Sci.*, 1994, **301**, 353-363.
86. Q. Ge, L. Wang and G. D. Billing, *Surf. Sci.*, 1992, **277**, 237-245.
87. D. Cheng, Z. Wei, Z. Zhang, P. Broekmann, A. N. Alexandrova and P. Sautet, *Angew. Chem. Int. Ed.*, 2023, **135**, e202218575.
88. Z. Zhang, Z. Wei, P. Sautet and A. N. Alexandrova, *J. Am. Chem. Soc.*, 2022, **144**, 19284–19293.
89. L. Vitos, A. Ruban, H. L. Skriver and J. Kollár, *Surf. Sci.*, 1998, **411**, 186-202.
90. J. Boettger, *Phys. Rev. B*, 1994, **49**, 16798.
91. V. Fiorentini and M. Methfessel, *J. Phys.: Condens. Matter*, 1996, **8**, 6525.
92. K. Chang, H. Zhang, J. G. Chen, Q. Lu and M.-J. Cheng, *Acs Catalysis*, 2019, **9**, 8197-8207.
93. K. Mathew, R. Sundararaman, K. Letchworth-Weaver, T. Arias and R. G. Hennig, *J. Chem. Phys.*, 2014, **140**, 084106.
94. R. Wu and L. Wang, *Phys. Chem. Chem. Phys.*, 2023, **25**, 2190-2202.
95. K. Mathew and R. Hennig, *Journal*, 2015.
96. R. Jinnouchi and A. B. Anderson, *Phys. Rev. B*, 2008, **77**, 245417.
97. A. J. Garza, A. T. Bell and M. Head-Gordon, *ACS Catal.*, 2018, **8**, 1490-1499.
98. J. D. Goodpaster, A. T. Bell and M. Head-Gordon, *J. Phys. Chem. Lett.*, 2016, **7**, 1471-1477.

99. Y. Cao, Q. Ge, D. J. Dyer and L. Wang, *J. Phys. Chem. B*, 2003, **107**, 3803-3807.
100. K. Spivey, J. I. Williams and L. Wang, *Chem. Phys. Lett.*, 2006, **432**, 163-166.
101. A. Groß and S. Sakong, *Chem. Rev.*, 2022, **122**, 10746-10766.
102. Y. Fang, S.-Y. Ding, M. Zhang, S. N. Steinmann, R. Hu, B.-W. Mao, J. M. Feliu and Z.-Q. Tian, *J. Am. Chem. Soc.*, 2020, **142**, 9439–9446.
103. D. C. Clary and L. Wang, *J. Chem. Soc., Faraday Trans.*, 1997, **93**, 2763-2767.
104. F. Chiter, D. Costa, V. Maurice and P. Marcus, *Corrosion Sci.*, 2022, **209**, 110658.
105. L. Xiao and L. Wang, *J. Phys. Chem. A*, 2004, **108**, 8605-8614.
106. L. Xiao, B. Tollberg, X. Hu and L. Wang, *J. Chem. Phys.*, 2006, **124**, 114309.
107. B. Wanjala, J. Lou, R. Loukrakpam, D. Mott, P. Njoki, B. Fang, M. Engelhard, H. R. Naslund, J. K. Wu, L. Wang, O. Malis and C. J. Zhong, *Chem. Mater.*, 2010, **22**, 4282-4294.
108. T. Pawluk, Y. Hirata and L. Wang, *J. Phys. Chem. B*, 2005, **109**, 20817-20823.
109. W. Zhang, Q. Ge and L. Wang, *J. Chem. Phys.*, 2003, **118**, 5793-5801.
110. W. Zhang, H. Zhao and L. Wang, *J. Phys. Chem. B*, 2004, **108**, 2140-2147.
111. L. Wang and Q. Ge, *Chem. Phys. Lett.*, 2002, **366**, 368-376.
112. W. Zhang, X. Ran, H. Zhao and L. Wang, *J. Chem. Phys.*, 2004, **121**, 7717-7724.
113. J. Lu, C. Aydin, N. D. Browning, L. Wang and B. C. Gates, *Catal. Lett.*, 2012, **142**, 1445-1451.
114. T. M. Onn, S. R. Gathmann, S. Guo, S. P. S. Solanki, A. Walton, B. J. Page, G. Rojas, M. Neurock, L. C. Grabow, K. A. Mkhoyan, O. A. Abdelrahman, C. D. Frisbie and P. J. Dauenhauer, *J. Am. Chem. Soc.*, 2022, **144**, 22113–22127.
115. G. Son, Y. Li, A. V. Shneidman, J. H. Han, M. Aizenberg, P. Sautet and J. Aizenberg, *Chem. Mater.*, 2022, **35**, 9505–9516.
116. X. Qin, J. Li, T.-W. Jiang, X.-Y. Ma, K. Jiang, B. Yang, S. Chen and W.-B. Cai, *Nat. Commun.*, 2024, **15**, 7509.
117. T. Sheng, W.-F. Lin, C. Hardacre and P. Hu, *J. Phys. Chem. C*, 2014, **118**, 5762-5772.
118. G. Kresse and J. Furthmüller, *Physical review B*, 1996, **54**, 11169.
119. P. E. Blöchl, *Phys. Rev. B*, 1994, **50**, 17953.
120. J. P. Perdew, K. Burke and M. Ernzerhof, *Phys. Rev. Lett.*, 1996, **77**, 3865.
121. H. J. Monkhorst and J. D. Pack, *Phys. Rev. B*, 1976, **13**, 5188.
122. V. Wang, N. Xu, J.-C. Liu, G. Tang and W.-T. Geng, *Comput. Phys. Commun.*, 2021, **267**, 108033.
123. K. Letchworth-Weaver and T. Arias, *Phys. Rev. B*, 2012, **86**, 075140.
124. M. Van den Bossche, E. Skúlason, C. Rose-Petruck and H. Jónsson, *J. Phys. Chem. C*, 2019, **123**, 4116-4124.
125. S. Ringe, N. G. Hörmann, H. Oberhofer and K. Reuter, *Chem. Rev.*, 2022, **122**, 10777-10820.
126. B. W. J. Chen, X. Zhang and J. Zhang, *Chem. Sci.*, 2023, **14**, 8338-8354.
127. K. Mathew, V. S. C. Kolluru, S. Mula, S. N. Steinmann and R. G. Hennig, *J. Chem. Phys.*, 2019, **151**, 234101.
128. Y. Wang, C. Teng, E. Begin, M. Bussiere and J. L. Bao, *J. Chem. Theory Comput.*, 2024, **20**, 6826–6847.
129. *J. Chem. Theory Comput.*, 2023, **19**, 5168-5175.
130. S. N. Steinmann and C. Michel, *ACS Catal.*, 2022, **12**, 6294-6301.
131. J. Huang, Y. Zhang, M. Li, A. Groß and S. Sakong, *J. Phys. Chem. Lett.*, 2023, **14**, 2354–2363.

132. J. J. Hinsch, A. Bouzid, J. C. Barker, J. J. White, F. Mortier, H. Zhao and Y. Wang, *J. Phys. Chem. C*, 2023, **127**, 19857–19866.
133. Z. Chai and S. Luber, *J. Chem. Theory Comput.*, 2024, **18**, 8214–8228.
134. A. J.-W. Wong, B. Tran, N. Agrawal, B. R. Goldsmith and M. J. Janik, *J. Phys. Chem. C*, 2024, **128**, 10837–10847.
135. A. Hagopian, M.-L. Doublet, J.-S. Filhol and T. Binninger, 2022, **18**, 1883–1893.
136. Y. Fang, R. Hu, J.-Y. Ye, H. Qu, Z.-Y. Zhou, S. Duan, Z.-Q. Tian and X. Xu, *Chem. Sci.*, 2023, **14**, 4905-4912.
137. L. Wang, R. M. Ore, P. K. Jayamaha, Z.-P. Wu and C.-J. Zhong, *Faraday Discuss.* , 2023, **242**, 429-442.
138. Y. Han, K. C. Lai, A. Lii-Rosales, M. C. Tringides, J. W. Evans and P. A. Thiel, *Surf. Sci.*, 2019, **685**, 48-58.
139. S. S. Tafreshi, A. Roldan and N. H. de Leeuw, *Surf. Sci.*, 2015, **637**, 140-148.
140. K. Klyukin, A. Zagalskaya and V. Alexandrov, *J. Phys. Chem. C*, 2018, **122**, 29350-29358.
141. A. Łukomska and J. Sobkowski, *J. Electroanal. Chem.*, 2004, **567**, 95-102.
142. J. Wandt, A. Freiberg, R. Thomas, Y. Gorlin, A. Siebel, R. Jung, H. A. Gasteiger and M. Tromp, *J. Mater. Chem.*, 2016, **4**, 18300-18305.